Rapid Enrichment and Detection of Extracellular Vesicles Enabled by CuS-Enclosed Microgels

Qiaoshi Jiang,[1,†] Yang Liu,[1,†] Linlin Wang,[2] Gary Brent Adkins,[2] Wenwan Zhong[1,2,*]

[1]Environmental Toxicology Graduate Program; [2]Department of Chemistry, University of California-Riverside, Riverside, CA 92521

[†] These authors contributed equally to the work.

ABSTRACT

Extracellular vesicles (EVs) are cell-derived membranous vesicles that exist in nearly all biological fluids including blood and urine; and carry a great number of cargo molecules such as protein, DNA, RNA and lipid. They may play important roles in cell-cell communication and modulation of pathological processes, which, however, are not yet well understood, calling for highly sensitive, specific, and rapid methods for EV detection and quantification in biological samples. Here, we report the CuS-enclosed microgels that not only help enrich EVs carrying specific protein markers from complex biomatrices, but also produce strong chemiluminescence (CL) to realize sensitive detection of the target EVs. A detection limit of 10^4 EV particles/mL was achieved with these microgels by targeting EV proteins like CD63 and HER2, with a dynamic range

up to 10^8 particles/mL. Direct detection of EVs in human serum and cell culture medium without tedious sample preparation was demonstrated, consuming much less sample compared to ELISA and Western Blot. We envision that our method will be valuable for quick quantification of EVs in biological samples, benefiting disease monitoring and functional study.

INTRODUCTION

Extracellular vesicles (EVs) are membrane-enclosed vesicles with sizes ranging from 50 to 200 nm; can be secreted by most cell types;[1,2] and are found in various body fluids like blood, bile and serum.[3] They carry miscellaneous molecular cargos including proteins, metabolites, and nucleic acids inherited from the parent cells;[2] and can transfer them to recipient cells, serving as a new route for cell-to-cell communication.[3] It is also believed that, EVs could mediate the tumor-related functions like formation, progression, and metastasis of malignant cells.[4] Besides, cells under pathological conditions could produce a large number of EVs loaded with unique cargoes reflecting disease development.[5,6] Thus, EVs are considered as promising markers in liquid biopsy for clinical diagnosis and prognosis. However, the abundance of the tumor-specific EVs in bio-fluids is very low, and their signals are buried within a large number of heterogeneous EVs from diverse sources, imposing great challenges to EV detection and quantification.

Enzyme-linked immunosorbent assays (ELISAs) and Western blots (WB) are the gold standards for detection of EVs through specific protein recognition.[7,8] Nanoparticle-tracking analysis (NTA) is another common method for EV analysis which measures the size distribution and particle concentration of clean EV samples.[9] But these methods all require purification and enrichment of EVs prior to detection, adding complexity to the assay.[10,11] In addition, without prior EV isolation, ELISA and WB could not differentiate the free and EV-bound proteins, making protein concentration detected not truly representative to that of the EVs.[6] Conventional isolation methods like ultracentrifugation consume large amounts of samples and yield low recovery. Recently, some advanced approaches and devices have been developed for EVs detection, such as DNA nanodevices,[9] electrochemistry,[12] microfluidics,[13] and surface enhanced Raman scattering.[14] These advancements have greatly enhanced researchers' capability to analyze EVs and identify the ones specifically related to pathological development. Still, methods that can avoid the labor-intensive EV purification steps and still provide specific and sensitive detection of the EV-bound proteins, are in high demand, for practical applications of EVs as the markers in liquid biopsy.

Herein, we report that the CuS-enclosed microgels can enable rapid EV isolation and sensitive quantification in complex biological samples. The microgels are designed to carry out dual functions in EV analysis: they can

facilitate *in situ* EV isolation through membrane filtration, while they contain a large number of Cu^{2+} ions per particle to produce strong chemiluminescence (CL) for EV detection. Only proteins on the EVs but not those freely suspended in samples are detected at very low concentrations with our method, which represents a beneficial tool for discovery of EV-based biomarkers and study of EV functions in disease development.

EXPERIMENTAL

Materials. N-(4-Aminobutyl)-N-ethylisoluminal (ABEI), sodium sulfide nonahydrate (SDS), potassium persulfate (KPS), N, N'-Methylenebisacrylamide (bis), acrylic acid (AA), allylamine (ALA) and N-isopropylacrylamide (NIPAM) were purchased from Sigma Aldrich. The biotinylated mouse anti-human ErbB2/ HER2 (Recombinant Monoclonal Human IgG_1 Clone Hu5), mouse anti-human CD63 (Clone mem-259), and biotinylated mouse anti-human CD63 (Clone NVG-2) was obtained from R&D systems, Sino Biological, and BioLegend, respectively. Horseradish peroxidase (HRP)-conjugated secondary antibody was from Cell Signaling Technology; and the streptavidin-HRP-conjugate was attained from Invitrogen. All other chemicals, including 1-(3-dimethylaminopropyl)-3-ethylcarbodiimide hydrochloride (EDC), and N-hydroxysulfosuccinimide (Sulfo-NHS), were purchased from ThermoFisher Scientific.

Cell culture. Human breast cell lines MCF-10A, MDA-MB-231 and SK-BR-3 were obtained from ATCC and cultured in the recommended media containing 1% penicillin streptomycin. MCF-10A cells were cultured in the Dulbecco's Modified Eagle Medium (DMEM)/Nutrient Mixture F-12 supplied with 5% horse serum, 0.1 µg/ml cholera toxin, 10 µg/ml insulin, 0.5 µg/ml hydrocortisone, and 20 ng/ml epidermal growth factor (EGF). MDA-MB-231 and SK-BR-3 cells were cultured in DMEM supplied with 10% and 20% fetal bovine serum (FBS), respectively. All cell lines were maintained at 37 °C in a humidified 5% CO_2 incubator and routinely screened for Mycoplasa contamination.

EV preparation. EV harvest was carried out by a Sorvall™ ST 16 Centrifuge (Thermofisher Scientific) and an Optima XPN-80 ultracentrifuge (Beckman Coulter). The medium was replaced with the EV-depleted culture medium after the cells reached a confluency of 75%. The cells were cultured for 24-48 hours in this medium, which was then centrifuged at 500 g for 15 min to sediment the cells, and another 20-min centrifugation at 15,000 g to remove the remaining cellular debris. Next, the medium was ultra-centrifuged at 110,000 g for 70 min to harvest the EVs released by the cells. The EV pellet was washed once and resuspended in the freshly prepared 1× DPBS. Particle concentration in the EV solution was measured by NTA with the NanoSight NS300 (Malvern Instruments). The EV solution was used within three day of preparation.

Microgel fabrication and antibody conjugation. Fabrication of the hydrogel microparticles followed the procedure reported previously with some modification.[15] In a typical procedure, 0.152 g of NIPAM, 0.030 g bis, 0.0225 g SDS and 47.5 µL AA were first dissolved with 23.5 mL of DI water in a 50 mL three-neck round bottom flask and stirred for 30 minutes under nitrogen. Secondly, the solution was heated to 70 °C, and 0.02 g KPS in 1.5 mL of water were injected into the flask to initiate the reaction. The reaction solution became milky within 10 minutes. After 10 minutes, 50 µL of ALA was injected and the solution became yellowish. The reaction continued for 4 hours. The product was cleaned up by dialysis against DI water for 2 days with frequent water changing using a 12-14 kDa dialysis membrane tubing (SpectrumLab), and stored at room temperature.

To encapsulate the CuS nanoparticles, the microgel stock was diluted with water to a final volume of 24 mL, in which the final concentration of the -COOH group was about 3 mM. $Cu(NO_3)_2$ was then added to a final concentration of 1.5 mM. The pH was adjusted to 5.6 with 1 M NaOH and the solution was stirred under room temperature for overnight. The next day, the solution was dialyzed against DI water for 2 days to remove the unbound Cu^{2+}. After dialysis, Na_2S was added to the solution at a final concentration of 1.5 mM. The solution turned orange and the reaction continued for 1 hour before being dialyzed against water to remove the free sulfide. The final product solution was kept at 4 °C.

Streptavidin was conjugated to the CuS-enclosed microgel by EDC/Sulfo-NHS. In brief, 10 µl of EDC at 0.4 mg/mL, 10 µL of Sulfo-NHS at 1.1 mg/mL, and 20 µL of streptavidin at 1 mg/mL were added to 160 µL of the MES buffer (50 mM MES, 0.15M NaCl, pH=6); and the mixture reacted for 15 minutes at room temperature. Then, 20 µL of this mixture was added to 1 ml of the CuS-enclosed microgel solution (10^{12} particles/ml), mixed well and reacted for 2 hours at room temperature. Afterwards, the solution was centrifuged at 500 g for 30 minutes to pass through the Amicon Ultra centrifugal filter (Sartorius Stedim Biotech) and remove the free streptavidin. The streptavidin-conjugated CuS-enclosed microgels were collected on top of the filter.

Microgel characterization. Transmission electron microscopy (TEM) images were recorded on a JEOL JEM-2100 transmission electron microscope at an acceleration voltage of 200 kV. UV−vis absorption spectra were collected using a spectrophotometer (Cary-100, Agilent Technologies). X-ray photoelectron spectroscopy (XPS) was performed using a Kratos AXIS ULTRADLD XPS system equipped with an Al Kα monochromated X-ray source and a 165-mm mean radius electron energy hemispherical analyzer.

EVs quantification with CuS-enclosed microgel. EV detection started by incubating 100 µL of the streptavidin-labeled CuS-enclosed microgel with 0.8 µL of the biotinylated antibody (5 µg/ml) for 1 hour. Then, 100 µL of the antibody-labeled microgel was added to 100 µL of the EV-containing sample and

incubated for 4 hours with gentle agitation. Followed, the reaction mixture was applied to the 0.45-μm Corning™ Costar™ Spin-X™ centrifuge tube filter and centrifuged at 14,000 g for 2 min. The free microgel particles were washed away with 800 μL of 1×PBS. At last, 100 μL of 1 M HNO_3 was added to the membrane to dissolve the CuS nanoparticles enclosed in the microgel; and the released Cu^{2+} was collected in the filtrate by another 2-min centrifugation. The pH of the filtrate was adjusted to 11 by adding 1 M NaOH, to which 10 μL of ABEI and 50 μL of H_2O_2 were injected to generate chemiluminescence (CL). The CL signal was monitored continuously for 120s under the luminescence mode in a GloMax®-Multi+ Microplate Reader (w/ dual injectors, Promega); and only the stable signal at the emission plateau was taken for analyte quantification.

EV quantification with ELISA. A 96-well plate was first incubated with the EV solution (50 μL per well) for 12 hours at 4 ℃. After washed with 1×PBS for three times, the plate was blocked at room temperature with 5% milk (100 μL per well) for 4 hours. After blocking, each well was washed twice with 1×PBS, before 100 μL of 0.5 μg/mL biotinylated anti-Human CD63 antibody in 1% BSA was added and incubated at room temperature for 2 hours. The free antibody was then removed by four washes with 1×PBS, before an aliquot (100 μL per well) of 1:20,000 dilution of the HRP-conjugated secondary antibody in 5% milk was added and incubated at room temperature for another hour. Then each well was washed twice with 1×PBS and incubated with the SuperSignal™ West Pico

PLUS Chemiluminescent Substrate (ThermoFisher) for 15 minutes before CL measurement.

RESUTLS AND DISCUSSION

CuS-enclosed microgel (CuS-MG) for EV isolation and detection. Reported EV concentration range from 10^4 and 10^{12} vesicles/mL in plasma,[16] but not all EVs are tumor-specific and suitable to be cancer markers in liquid biopsy. During early disease development, the number of diseased cells is low, so is the concentration of the EVs originated from such cells, thus demanding highly sensitive methods for their detection. Other obstacles for EV analysis in biofluids are their small sizes and the presence of the interfering matrix components, both requiring EV enrichment and isolation prior to detection. In the present work, we solve these difficulties by the hydrogel microparticles, i.e. microgels (MGs) that encapsulate numerous CuS nanoparticles, as illustrated in Scheme 1. The MGs are fabricated through copolymerization of AA, NIPAM and ALA.[17] Each MG particle carries a high density of carboxyl groups in the polymer network originated from AA, which can coordinate with a large number of divalent ions like Zn^{2+} and Cu^{2+} to facilitate their encapsulation in the MG particle in the form of sulfide nanoparticles (NPs) (Gray inset of Scheme 1).[17] The NPs possesses high stability in solutions, but can release the encapsulated cations upon stimulation for signaling purpose. Cu^{2+} has been reported to be able to catalyze

strong emission from the traditional CL systems, such as luminol-H_2O_2 and ABEI-H_2O_2,[18] through the Fenton-like reaction that produces the highly reactive species of OH•.[19] CL requires no exciting light source, and is generated through specific chemical reactions. Thus, CL-based detection experiences low or no background, rendering high signal-to-noise ratio and high sensitivity.[20,21] Moreover, in our design, each of the CuS-MG can release many Cu^{2+} ions to produce strong CL, realizing effective signal amplification to detect the low-abundance EVs in samples.

Additionally, the size of the MGs can be controlled by adjusting the monomer composition. Therefore, we can fabricate the MGs with the desired sizes that they could freely pass through a wide-bore filter before EV binding (Process ***b*** in Scheme 1) but being retained by the filter after binding to the target EVs (Process ***a*** in Scheme 1). Either an EV carrying multiple copies of the target protein could link several MG particles together; or one MG particle may bind to several EVs, both increasing the overall size of the MGs and preventing them from passing through the filter. Although filtration is one of the conventional approaches for EV isolation,[22] filters with ultrafine pores are employed which have to be handled by high pressure or strong vacuum. Or, a series of filters are assembled into sophisticated devices.[23,24] The high forces involved could be detrimental to EV structures; and the specialized devices are not widely accessible. In contrast, our design induces aggregation of the signaling units of

MGs in the presence of the target EVs, and only the wide-bore filters that can be handled with a simple table-top centrifuge are used, greatly simplifying the procedure and the technical demand. The retained MGs can then be digested by acid to release the encapsulated Cu^{2+} ions and catalyze CL emission, enabling sensitive EV detection.

MG preparation and characterization. A proper MG size is very important for the success of our design. We control the size of the MG by fine tuning the relative contents of the negatively charged carboxyl groups from AA and the positively charged amine groups from the crosslinker ALA. We adjusted the concentration of ALA in MG synthesis and added it at various time points after copolymerization between AA and NIPAM was initiated (Supporting Information Table S1). We learned from the results that, by keeping all other reaction conditions the same, adding ALA at 10 min instead of 1 hour after the initial polymerization reduced the size of MG from ~ 500 nm to ~ 300 nm, which further decreased to ~ 100 nm by increasing the ALA amount by 4 folds. Increasing the mass of the crosslinker could form a more rigid gel network, limiting MG expansion and thus its size. Shortening the duration of the initial polymerization step may have increased the proportion of ALA to be incorporated into the polymer network, thus neutralizing more carboxyl groups and suppressing gel expansion. With ALA added at only 10 minutes after the

initial copolymerization, the amine groups may be closer to the surface of MG to facilitate conjugation of the target-recognizing molecules like antibody.

Although ALA partially neutralized the carboxyl groups, the surface potential of the MG was measured to be around -20 mV (Supporting Information Figure S1). Both the amine and carboxyl groups could form strong coordination with Cu^{2+}, which was exploited to form CuS NPs within each MG particle via the sequential addition of Cu^{2+} and S^{2-}. TEM images (Figure 1a&b) clearly showed that ultrafine NPs were enclosed inside each of the MG particles. X-ray photoelectron spectroscopy (XPS) also confirmed the presence of Cu in those particles by displaying the Cu 2p peaks at 932.7 eV and 952.3 eV (Fig. 1c). The peak intensities from the 500-nm MG were higher than the two smaller ones, indicating their higher Cu content per unit mass of the MG (Fig. 1c). The 2p peaks for S were also found, although their signal-to-noise ratios in all three MGs were very low (Figure S1B). The Cu^{2+} content in each type of MG was quantified by ICP-AES (Figure 1d), and the results agreed with the observation shown in Figure 1c: larger the size of the MG, more Cu^{2+} were enclosed in each gel particle. While only $(1.7 \pm 0.06)\times10^4$ (n = 3) Cu^{2+} ions were enclosed in each of the 100-nm MG in average, this concentration increased to $(6.4 \pm 0.03)\times10^5$ (n = 3) in the 500-nm MG.

CL generation by CuS-enclosed MG (CuS-MG). By enclosing numerous CuS NPs inside each MG, CL emission can be directly catalyzed by the CuS NPs,

owing to the high porosity of the hydrogel structure and the high surface activity of the ultrafine NPs. Alternatively, free Cu^{2+} ions can be released from the MG by acid digestion and act as catalyst. We compared the CL signals resulted from these two approaches using 8 pM – 435 pM of the 300-nm MG. As shown in Figure 2a, with the same amount of MG, the signal from the freed Cu^{2+} after acid digestion was at least two times higher than that from the intact CuS-MG. Larger differences were observed with higher MG concentrations. This is probably because the CuS NPs catalyzed the CL production only through the Cu^{2+} ions on the NP surface, with those inside the NP core not participating. In addition, both reactants, i.e. H_2O_2 and ABEI, need to diffuse into the MG network to be close to the CuS NPs, which generates a barrier for the reaction. Thus, acid digestion was employed in the following work for CL production. The digestion was proved to be nearly complete within 15 minutes without damaging the membrane (Supporting Information Figure S3a). Typically, CL emission from the released Cu^{2+} was monitored for 120 s, within which the CL signal rapidly increased and reached a plateau within 60 s (Supporting Information Figure S2). The stable signal at the plateau was then recorded for target quantification.

We evaluated the performance of CL generation by the 100-, 300-, and 500-nm MGs, and compared it with HRP, the gold standard used in immunoassays for CL production. Agreeing with their higher Cu contents than the smaller particles, the largest, 500-nm MG produced the strongest CL if the particle

concentration was the same. Both the 300- and 500-nm MG outperformed HRP in catalyzing CL emission with 10 mM H_2O_2 and 0.5 mM ABEI: using the 300- and 500-nm MGs, as low as 0.0038 and 0.1 pM of the MG particles, respectively, could be detected, while the limit of detection (LOD) of HRP was only 0.1 nM (Figure 2b). The detection performance of the 100-nm MG was comparable to that of HRP due to the lower content of the enclosed Cu^{2+}. The curves plotting CL intensity vs. MG concentration all exhibited a hyperbolic shape, showing slower increase in CL within the lower MG concentration range. Such a feature agrees with the previous reports on using Cu^{2+}-based material for CL production;[25] and may be attributed to the two-step catalytic process of the Cu^{2+}-H_2O_2 system:[19,26] firstly Cu^{2+} is reduced to Cu^{+} by H_2O_2, which is the rate-limiting step, and secondly Cu^{+} is cycled back to Cu^{2+} by H_2O_2-mediate oxidation, accompanied by production of the highly reactive species, hydroxyl radical, responsible for strong CL emission. Thus, higher Cu^{2+} concentration significantly speeds up the rate-limiting step to attain a comparable rate as the second reaction step, causing more rapid increase in CL with unit increase in MG concentration. In the following study, only the 300- and 500-nm MG were employed because of their superior detectability compared to HRP.

EV quantification with CuS-MG. In our design, the MGs should not be retained by the filter before binding to the target EVs; but their sizes will be larger than the filter pores after binding. For rapid filtration assisted by a table-

top centrifuge, the typical filter devices have the pore size of 0.65, 0.45 and 0.22 µm. Since this work employed the MG with an average diameter of 300- or 500-nm, the filter with a pore size of 0.45 µm was selected and the filter passing rates of the two MGs were compared. More than 90% of the 300-nm MGs could pass through the 0.45-µm centrifugal filter by a 2-min gentle centrifugation with a bench-top microcentrifuge. This ratio was slightly higher than that of the 500-nm MGs (Supporting Information Figure S3b). The following assays thus all employed the 300-nm MG particles.

The 300-nm MGs were conjugated with streptavidin to anchor the biotinylated antibodies targeting various EV proteins. Streptavidin was activated with EDC-sulfo-NHS and linked to the amine groups on the MG. Although the MGs also carried carboxyl groups, treating them with the activation reagents led to severe aggregations of MGs, reducing MG recovery after conjugation. Interestingly, lower concentrations of streptavidin used for conjugation led to more severe MG aggregation and lower MG recovery when using the 300k MWCO Spin filters to clean up the conjugated MG and remove the free streptavidin. Two µg/mL of streptavidin was the optimal concentration yielding the highest passing rate comparing with lower concentrations (Figure S3c).

The proof-of-principle work targeted the EVs carrying two specific surface proteins, CD63 and HER2. CD63 is a tetraspanin protein on EV surface and one of the universal EV markers. HER2 has been found to be present on the EVs

derived from certain tumor cells that carry over expression of HER2, and represents a tumor-specific marker. The biotinylated anti-CD63 or anti-HER2 IgG were anchored to the streptavidin-conjugated MG particles, the resultant of which were then mixed with samples containing standard EVs at various concentrations in 1×PBS. The solution was filtrated to remove the unbound MGs, and acid digestion was conducted to release the Cu^{2+} ions from the gel particles retained on top of the filter after EV binding, which in turn catalyzed CL emission from ABEI. The plot showed a linear relationship for both surface markers within the EV concentration range of 10^4 to 10^8 particles/mL (Figure 3a&b). The LOD was calculated to be $8.27\pm0.20\times10^2$ EV particles/mL for CD63, and $3.43\pm0.04\times10^3$ EV particles/mL for HER2, based on the 3σ method.

Detection of EVs in serum. The high sensitivity of our assay allows it to detect EVs in complex biological samples. We spiked the standard EVs into the 5× diluted EV-free serum; and 100 μL of the spiked serum was applied for our assay. Again, linear relationships between Log (CL) and Log (EV concentration) using either CD63 or HER2 as the target protein were observed (Figure 3c & d). The complex matrix of serum reduced the sensitivity for detection of the CD63-positive EVs by about 3 folds judged by the slope of the calibration curves (Fig. 3a & c), but interestingly the slope did not change much for detection of the HER2-positive EVs. As a result, the LOD for CD63- and HER2-based EV detection increased by about 13 and 7 folds, respectively. Still, such an LOD is lower than

what could be obtained by NTA (10^8 – 10^9 particles/mL) and ELISA (10^{10} particles/mL), as well as most of those reported in literature by far (Supporting Information Table S2)[12,13,27-37]. We also tested the recovery of EVs with our method by adding a known amount of the standard EVs to 100 µl of the EV-depleted serum. The percent recovery was calculated by dividing the detected EV concentration with the spiked concentration, and found to be between 96.9% and 99.7% with the various EV concentrations used (Table 1).

To briefly demonstrate the applicability of method in clinical testing, we applied it to evaluate the EV concentration in two clinical samples, one from a healthy individual and the other from a patient with early stage breast cancer. For each test, we only employed 1 µL of the raw serum sample, diluted it to 100 µL with 1×PBS, and mixed it well with the antibody-conjugated MG solution. The CL signals were compared between these two samples (Supporting Information Figure S4). The result indicated that, the CL signal from the CD63-positive EV in the serum of the healthy individual was higher than that from the cancer patient; while the signal from the HER2-positive EVs showed an opposite trend. Since CD63 is considered as a general marker for EVs and HER2 is used to mark EVs derived from tumor cells with HER2 overexpression, the relative signal intensity observed by our method reflects that, the patient serum used in this study contained a higher proportion of the EVs carrying the tumor-specific HER2 than the one collected from a healthy individual. Of course by testing two

clinical samples, we cannot conclude this could be a general observation between samples from breast cancer patients and healthy individuals. But numerous works analyzing the protein expression profiles on single EVs have reported the possibility of using the relative contents of EVs carrying different protein markers for disease diagnosis.[38-41] Compared to these techniques, our method provides a simpler approach to evaluate the relative contents by targeting various EV proteins with comparable sensitivity, enabling examination in a large collection of clinical samples for validation of such hypothesis.

Detection of EVs in cell culture medium. Upon the discovery of the possible functions of EVs in cell-cell communication, cancer metastasis, cell reprogramming, etc., intense works have been devoted to study the biogenesis of EVs from different cells of origin, and how their secretion could be stimulated by external factors.[42,43] [26-28]EV secretion by diverse cell lines is being examined extensively. The low sensitivity of the conventional methods like ELISA and WB makes it difficult to monitor EV secretion in the cell culture medium, which is often in mLs and contains low numbers of EVs if the number of cells are not adequate and the harvest duration is shorter than 24 hrs.[44] Ultracentrifugation or other tedious EV isolation methods are needed to enrich the EVs from the culture media into a much smaller volume for down-stream analysis. Because our method employs filtration to retain the EVs upon binding to the MG particles, and it is highly sensitive, it should be suitable for monitoring EV

secretion from stimulated cells without EV pre-concentration nor consumption of a large amount of cells.

To demonstrate this capability, we tested the EVs concentration in the culture media of three cell lines: the non-cancer cell line of MCF-10A, and the cancer cell lines of MDA-MB-231 and SK-BR-3. It has been reported that both MCF-10A and MDA-MB-231 have low HER2 expression and SK-BR-3 cells express a higher level of HER2 than the other two.[38,45] Only 100 μL of the cell culture medium was subject for EV quantification by the CuS-MG conjugated to either the anti-CD63 or anti-HER2 antibodies. The CL signals obtained from the EVs collected from these three cell lines were compared in Figure 4a. We can see that, the CL intensities resulted from the anti-CD63 MG were comparable among the three cell lines, but those from the anti-HER2 MG were quite different, with that from the SK-BR-3 cells being the highest, agreeing with its higher HER2 expression level than the other cell lines.

Interestingly, subjecting the CL data shown in Figure 4a to principle component analysis (PCA), we successfully differentiated the EVs secreted from different cell lines. On the resultant score plot (Figure 4b), the EVs from the two HER2-basal subtypes of breast cells (MCF-10A and MDA-MB-231) were clustered closely to each other, indicating their CD63 and HER2 expression profiles were similar; but were far away from the EVs secreted by SK-BR-3, which overly

expressed HER2.[46] This proves that, by targeting dual protein markers, our method is capable to differentiate EVs originated from different cells.

We also employed ELISA to quantify CD63 in these samples, and found a very strong linear relationship with an R value of 0.99 and a significance value < 0.001 between the protein contents and the CL signal obtained by our method (Figure 4c), well supporting that the CL signal is proportional to the content of EV proteins secreted by the cells. However, to obtain the ELISA result, a total of 45-75 mL culture medium which was needed to culture about 4×10^7 - 6×10^7 cells were ultracentrifuged to obtain the precipitated EVs prior to detection. Such a sample consumption is 450-750 times more than what was used in our method (Supporting Information Figure S5), which can enrich the EVs on top of the filter by the aid of the CuS-MG and provide high detection sensitivity to assess the EV content in a very small volume of the culture medium. In addition, our method ensures detection of proteins on EVs instead of the free proteins, because free proteins cannot serve as the bridges to link different MGs and induce MG aggregation: negligible signals from the MG particles were obtained with 0.19-19.23 fM of protein (Supporting Information Figure S6).

CONCLUSIONS

To summarize, we have developed a method that utilize the CuS-enclosed MG and membrane filters for sensitive and fast detection of EVs in buffer, cell

culture medium and biospecimen like serum. The size of the MG allows rapid EV purification and enrichment through filtration, because they aggregate upon binding to EVs carrying specific surface proteins. The large number of Cu^{2+} enclosed in each MG generate highly intense CL with few numbers of EVs. As low as 10^4 particles/mL EVs were detected with our method targeting two different EV surface proteins; and its applicability for EV detection in serum or in culture medium was demonstrated.

With its high detection speed and high sensitivity, our method will benefit study of EV functions and biogenesis, as well as be suitable for disease monitoring based on EV markers. Definitely future studies should be conducted to target a wide scope of the marker proteins on EVs. With the selection of the appropriate EV- and tumor-specific markers, evaluation of EV expression in more clinical samples than used in this proof-of-principle study is desired to confirm the potential of our method in cancer diagnosis and prognosis.

ASSOCIATED CONTENT

Supporting Information

The Supporting Information is available free of charge on the ACS Publications website: additional figures for material characterization; the CL emission kinetic curve; optimization of acid digestion conditions; EV quantification in clinical samples; sample consumption comparison between our method and traditional

methods; detection of free proteins with our method; and tables for fabrication optimization and existing relevant reports for EV detection methods.

ACKNOWLEDGMENT

This work was supported by National Institutes of Health grants R01- CA188991 and University of California Cancer Coordinating Committee, Grant ID #CRR-19585695, to W. Z. We are also grateful to the support from the Research Training Grant in Environmental Toxicology from the National Institute of Environmental Health Sciences (T32ES018827) to G. B. A.; and the support from the Environmental Toxicology Program fund for Q. J. Kind advices in cell culture and EV extraction provided by Dr. Wei Yan and Dr. Emily Wang are highly appreciated.

References

(1) Théry, C.; Zitvogel, L.; Amigorena, S. *Nature reviews immunology* **2002**, *2*, 569.
(2) He, C.; Zheng, S.; Luo, Y.; Wang, B. *Theranostics* **2018**, *8*, 237.
(3) Nedaeinia, R.; Manian, M.; Jazayeri, M.; Ranjbar, M.; Salehi, R.; Sharifi, M.; Mohaghegh, F.; Goli, M.; Jahednia, S.; Avan, A. *Cancer gene therapy* **2017**, *24*, 48.
(4) Rajagopal, C.; Harikumar, K. *Frontiers in oncology* **2018**, *8*, 66.
(5) Huang, T.; Deng, C.-X. *International journal of biological sciences* **2019**, *15*, 1.
(6) Vlassov, A. V.; Magdaleno, S.; Setterquist, R.; Conrad, R. *Biochimica et Biophysica Acta (BBA)-General Subjects* **2012**, *1820*, 940-948.
(7) Li, A.; Zhang, T.; Zheng, M.; Liu, Y.; Chen, Z. *Journal of hematology & oncology* **2017**, *10*, 175.

(8) Yu, S.; Liu, C.; Su, K.; Wang, J.; Liu, Y.; Zhang, L.; Li, C.; Cong, Y.; Kimberly, R.; Grizzle, W. E. *The Journal of Immunology* **2007**, *178*, 6867-6875.
(9) He, D.; Ho, S.-L.; Chan, H.-N.; Wang, H.; Hai, L.; He, X.; Wang, K.; Li, H.-W. *Analytical chemistry* **2019**, *91*, 2768-2775.
(10) Cheruvanky, A.; Zhou, H.; Pisitkun, T.; Kopp, J. B.; Knepper, M. A.; Yuen, P. S.; Star, R. A. *American Journal of Physiology-Renal Physiology* **2007**, *292*, F1657-F1661.
(11) Zarovni, N.; Corrado, A.; Guazzi, P.; Zocco, D.; Lari, E.; Radano, G.; Muhhina, J.; Fondelli, C.; Gavrilova, J.; Chiesi, A. *Methods* **2015**, *87*, 46-58.
(12) Doldán, X.; Fagúndez, P.; Cayota, A.; Laíz, J.; Tosar, J. P. *Analytical chemistry* **2016**, *88*, 10466-10473.
(13) Xu, H.; Liao, C.; Zuo, P.; Liu, Z.; Ye, B.-C. *Analytical chemistry* **2018**, *90*, 13451-13458.
(14) Stremersch, S.; Marro, M.; Pinchasik, B. E.; Baatsen, P.; Hendrix, A.; De Smedt, S. C.; Loza-Alvarez, P.; Skirtach, A. G.; Raemdonck, K.; Braeckmans, K. *Small* **2016**, *12*, 3292-3301.
(15) Zhang, J.; Xu, S.; Kumacheva, E. *Journal of the American Chemical Society* **2004**, *126*, 7908-7914.
(16) Coumans, F. A. W.; Brisson, A. R.; Buzas, E. I.; Dignat-George, F.; Drees, E. E. E.; El-Andaloussi, S.; Emanueli, C.; Gasecka, A.; Hendrix, A.; Hill, A. F.; Lacroix, R.; Lee, Y.; van Leeuwen, T. G.; Mackman, N.; Mäger, I.; Nolan, J. P.; van der Pol, E.; Pegtel, D. M.; Sahoo, S.; Siljander, P. R. M., et al. *Circulation Research* **2017**, *120*, 1632-1648.
(17) Liu, Y.; Wang, Y.-M.; Sedano, S.; Jiang, Q.; Duan, Y.; Shen, W.; Jiang, J.-H.; Zhong, W. *Chem. Commun.* **2018**, *54*, 4329-4332.
(18) Zhang, S.; Zhong, H.; Ding, C. *Analytical chemistry* **2008**, *80*, 7206-7212.
(19) Lyu, L.; Zhang, L.; Hu, C. *Chemical Engineering Journal* **2015**, *274*, 298-306.
(20) Adcock, J. L.; Barnett, N. W.; Francis, P. S. In *Encyclopedia of Analytical Science (Third Edition)*, Worsfold, P.; Poole, C.; Townshend, A.; Miró, M., Eds.; Academic Press: Oxford, 2019, pp 412-419.
(21) Roda, A.; Guardigli, M. *Anal. Bioanal. Chem.* **2012**, *402*, 69-76.
(22) Merchant, M. L.; Powell, D. W.; Wilkey, D. W.; Cummins, T. D.; Deegens, J. K.; Rood, I. M.; McAfee, K. J.; Fleischer, C.; Klein, E.; Klein, J. B. *PROTEOMICS–Clinical Applications* **2010**, *4*, 84-96.
(23) Konoshenko, M. Y.; Lekchnov, E. A.; Vlassov, A. V.; Laktionov, P. P. *BioMed research international* **2018**, *2018*.
(24) Li, P.; Kaslan, M.; Lee, S. H.; Yao, J.; Gao, Z. *Theranostics* **2017**, *7*, 789.
(25) Khajvand, T.; Akhoondi, R.; Chaichi, M. J.; Rezaee, E.; Golchoubian, H. *Journal of Photochemistry and Photobiology A: Chemistry* **2014**, *282*, 9-15.
(26) Nichela, D. A.; Berkovic, A. M.; Costante, M. R.; Juliarena, M. P.; Einschlag, F. S. G. *Chemical engineering journal* **2013**, *228*, 1148-1157.

(27) Jeong, S.; Park, J.; Pathania, D.; Castro, C. M.; Weissleder, R.; Lee, H. *ACS nano* **2016**, *10*, 1802-1809.
(28) Xu, R.; Fitts, A.; Li, X.; Fernandes, J.; Pochampally, R.; Mao, J.; Liu, Y.-M. *Anal. Chem.* **2016**, *88*, 10390-10394.
(29) Zhang, P.; He, M.; Zeng, Y. *Lab on a Chip* **2016**, *16*, 3033-3042.
(30) He, F.; Liu, H.; Guo, X.; Yin, B.-C.; Ye, B.-C. *Anal. Chem.* **2017**, *89*, 12968-12975.
(31) Wang, Y.-M.; Liu, J.-W.; Jiang, J.-H.; Zhong, W. *Analytical and Bioanalytical Chemistry* **2017**, *409*, 4225-4232.
(32) Wang, Y.-M.; Liu, J.-W.; Adkins, G. B.; Shen, W.; Trinh, M. P.; Duan, L.-Y.; Jiang, J.-H.; Zhong, W. *Anal. Chem.* **2017**, *89*, 12327-12333.
(33) Xia, Y.; Liu, M.; Wang, L.; Yan, A.; He, W.; Chen, M.; Lan, J.; Xu, J.; Guan, L.; Chen, J. *Biosens. Bioelectron.* **2017**, *92*, 8-15.
(34) Dong, H.; Chen, H.; Jiang, J.; Zhang, H.; Cai, C.; Shen, Q. *Anal. Chem.* **2018**, *90*, 4507-4513.
(35) He, F.; Wang, J.; Yin, B.-C.; Ye, B.-C. *Anal. Chem.* **2018**, *90*, 8072-8079.
(36) Gao, M.-L.; He, F.; Yin, B.-C.; Ye, B.-C. *Analyst* **2019**, *144*, 1995-2002.
(37) Boriachek, K.; Masud, M. K.; Palma, C.; Phan, H.-P.; Yamauchi, Y.; Hossain, M. S. A.; Nguyen, N.-T.; Salomon, C.; Shiddiky, M. J. *Anal. Chem.* **2019**, *91*, 3827-3834.
(38) Shen, W.; Guo, K.; Adkins, G. B.; Jiang, Q.; Liu, Y.; Sedano, S.; Duan, Y.; Yan, W.; Wang, S. E.; Bergersen, K. *Angewandte Chemie International Edition* **2018**, *57*, 15675-15680.
(39) Lee, K.; Fraser, K.; Ghaddar, B.; Yang, K.; Kim, E.; Balaj, L.; Chiocca, E. A.; Breakefield, X. O.; Lee, H.; Weissleder, R. *ACS nano* **2018**, *12*, 494-503.
(40) Ji, Y.; Qi, D.; Li, L.; Su, H.; Li, X.; Luo, Y.; Sun, B.; Zhang, F.; Lin, B.; Liu, T. *Proceedings of the National Academy of Sciences* **2019**, *116*, 5979-5984.
(41) Zhang, P.; Zhou, X.; He, M.; Shang, Y.; Tetlow, A. L.; Godwin, A. K.; Zeng, Y. *Nature biomedical engineering* **2019**, *3*, 438-451.
(42) Im, E.-J.; Lee, C.-H.; Moon, P.-G.; Rangaswamy, G. G.; Lee, B.; Lee, J. M.; Lee, J.-C.; Jee, J.-G.; Bae, J.-S.; Kwon, T.-K. *Nature communications* **2019**, *10*, 1387.
(43) Benedikter, B. J.; Wouters, E. F.; Savelkoul, P. H.; Rohde, G. G.; Stassen, F. R. *Journal of Toxicology and Environmental Health, Part B* **2018**, *21*, 142-160.
(44) Théry, C.; Amigorena, S.; Raposo, G.; Clayton, A. *Current protocols in cell biology* **2006**, *30*, 3.22. 21-23.22. 29.
(45) Fang, S.; Tian, H.; Li, X.; Jin, D.; Li, X.; Kong, J.; Yang, C.; Yang, X.; Lu, Y.; Luo, Y. *PLoS One* **2017**, *12*, e0175050.
(46) Subik, K.; Lee, J.-F.; Baxter, L.; Strzepek, T.; Costello, D.; Crowley, P.; Xing, L.; Hung, M.-C.; Bonfiglio, T.; Hicks, D. G. *Breast cancer: basic and clinical research* **2010**, *4*, 117822341000400004.

Figure Captions

Scheme 1. Schematic illustration of CuS-MG synthesis (upper gray panel) and the CuS-MG based assay for EV quantification (lower panel).

Figure 1. Characterization of CuS-MG. TEM images of CuS-MG with an average diameter of a) 300 nm and b) 500 nm. c) XPS (Cu 2p) element analysis of CuS-MG. d) ICP-AES quantification of Cu^{2+} concentration in three CuS-MG.

Figure 2. a) Chemiluminescence of ABEI-H_2O_2 system stimulated by the 300-nm CuS-MG or Cu^{2+} released from it after acid digestion; b) comparison of chemiluminescence of ABEI-H_2O_2 system stimulated by HRP and CuS-MG with an average diameter of 100, 300 and 500 nm. [ABEI] = 0.5 mM, [H_2O_2] = 1 mM, in 1× PBS (pH = 7.4) for HRP or in a basic solution (pH = 11) for CuS-MG.

Figure 3. Quantification of EV concentrations with the 300-nm CuS-MG in 1× PBS or Serum. Calibration curves in 1×PBS using a) anti-CD63, b) anti-HER2; and in serum using c) anti-CD63 or d) anti-HER2. CL_0 = chemiluminescence without EVs. [ABEI] = 0.5 mM, [H_2O_2] =1 mM, pH=11.

Figure 4. Detection of cell released EVs using CuS-MG. The cell culture medium was collected from three cell lines: MCF-10A, MDA-MB-231 and SK-BR-3. a) Chemiluminescence resulted from EV detection in the culture media of three cell lines targeting CD63 and anti-HER2; b) PCA plot using the

chemiluminescence data shown in a); c) Linear correlation between CD63 quantification results obtained by ELISA and the chemiluminescent signals from CuS-MG in our assay targeting CD63. [ABEI] = 0.5 mM, [H_2O_2] = 1 mM, pH=11.

Table 1. Percent recovery of spiked EVs in serum samples. EV depleted serum was spiked with different number of EVs and measured by CuS-MG. The data is shown as mean ± %RSD (n=3).

Scheme 1.

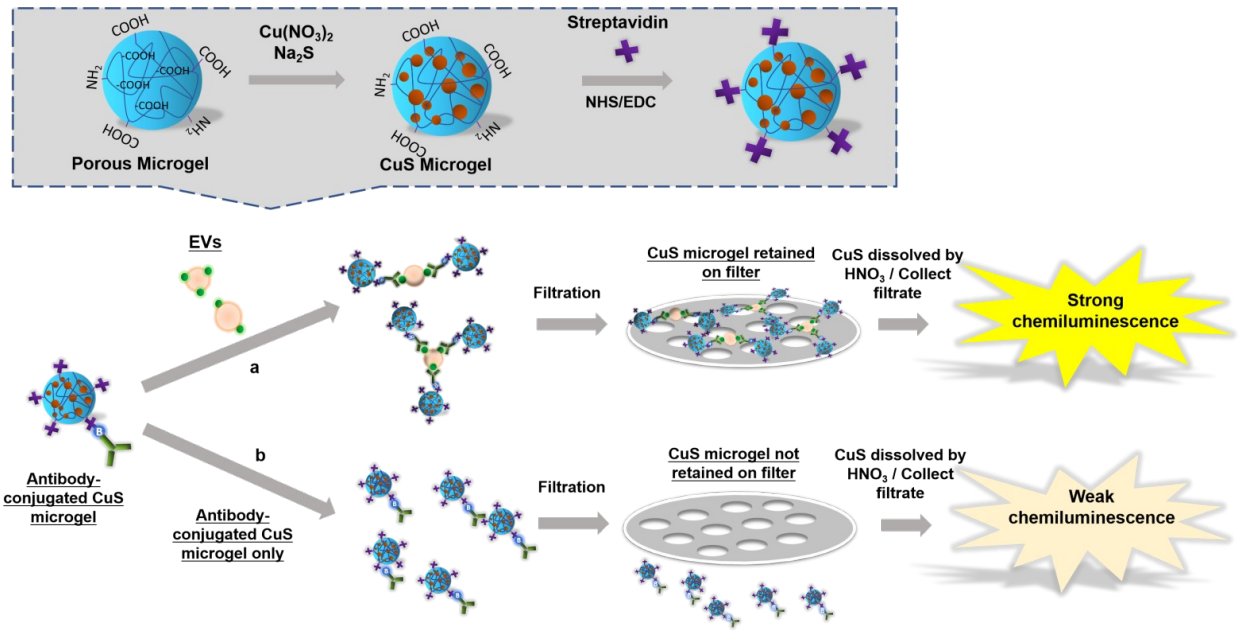
Cu(NO3)2
Na2S
Streptavidin
NHS/EDC
Porous Microgel
CuS Microgel
EVs
a
b
Antibody-conjugated CuS microgel
Antibody-conjugated CuS microgel only
Filtration
Filtration
CuS microgel retained on filter
CuS microgel not retained on filter
CuS dissolved by HNO3 / Collect filtrate
CuS dissolved by HNO3 / Collect filtrate
Strong chemiluminescence
Weak chemiluminescence

Figure 1.

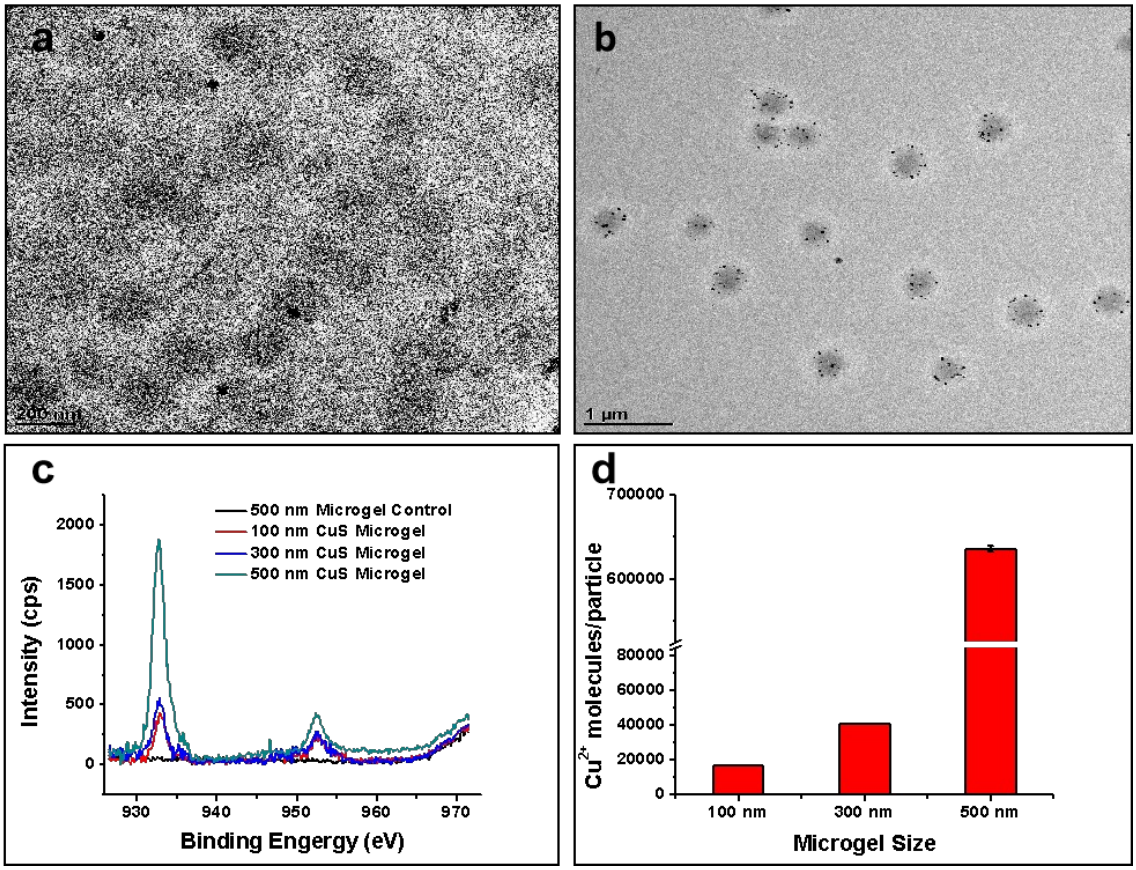
a
200 nm
b
1 μm
c
500 nm Microgel Control
100 nm CuS Microgel
300 nm CuS Microgel
500 nm CuS Microgel
Intensity (cps)
2000
1500
1000
500
0
930
940
950
960
970
Binding Engergy (eV)
d
700000
600000
80000
60000
40000
20000
0
Cu2+ molecules/particle
100 nm
300 nm
500 nm
Microgel Size

Figure 2.

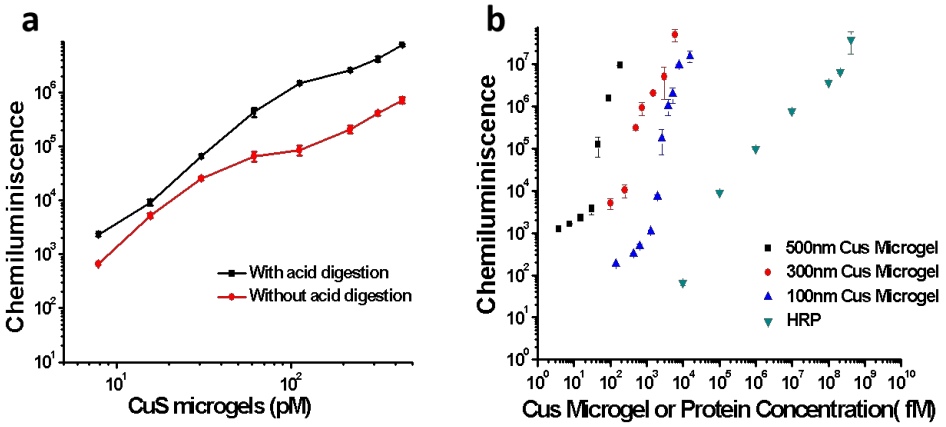
a
Chemiluminiscence
CuS microgels (pM)
With acid digestion
Without acid digestion
b
Chemiluminiscence
Cus Microgel or Protein Concentration(fM)
500nm Cus Microgel
300nm Cus Microgel
100nm Cus Microgel
HRP

Figure 3.

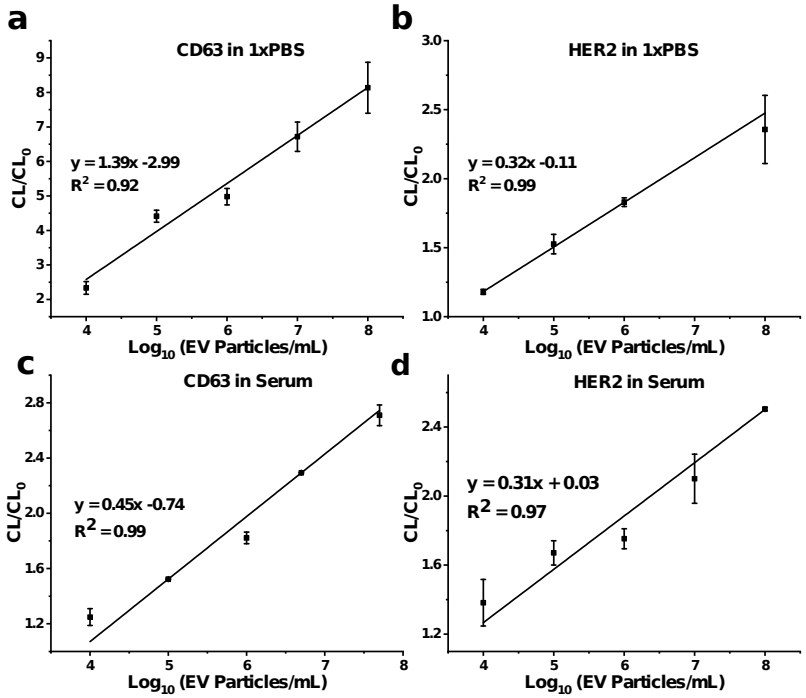
a
CD63 in 1xPBS
y = 1.39x -2.99
R2 = 0.92
CL/CL0
Log10 (EV Particles/mL)
b
HER2 in 1xPBS
y = 0.32x -0.11
R2 = 0.99
CL/CL0
Log10 (EV Particles/mL)
c
CD63 in Serum
y = 0.45x -0.74
R2 = 0.99
CL/CL0
Log10 (EV Particles/mL)
d
HER2 in Serum
y = 0.31x + 0.03
R2 = 0.97
CL/CL0
Log10 (EV Particles/mL)

Figure 4.

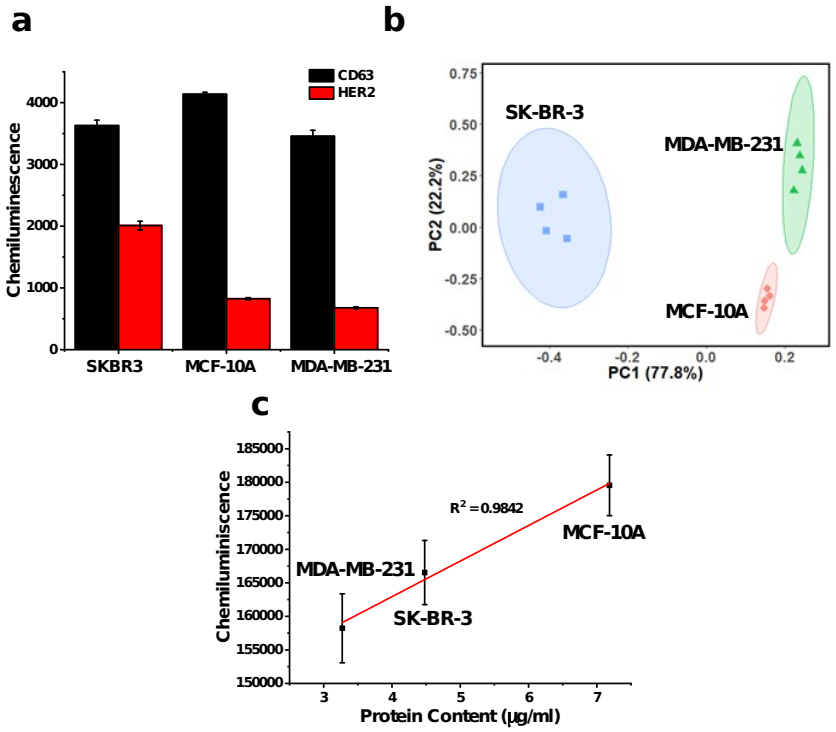

Table 1.

EV Spiked in Serum (Particles/mL)	Recovery Rate
5×10^6	96.9 ± 3.4
2.5×10^6	97.5 ± 2.7
5×10^5	99.7 ± 2.0